

# RSC Advances



This is an *Accepted Manuscript*, which has been through the Royal Society of Chemistry peer review process and has been accepted for publication.

*Accepted Manuscripts* are published online shortly after acceptance, before technical editing, formatting and proof reading. Using this free service, authors can make their results available to the community, in citable form, before we publish the edited article. This *Accepted Manuscript* will be replaced by the edited, formatted and paginated article as soon as this is available.

You can find more information about *Accepted Manuscripts* in the [Information for Authors](#).

Please note that technical editing may introduce minor changes to the text and/or graphics, which may alter content. The journal's standard [Terms & Conditions](#) and the [Ethical guidelines](#) still apply. In no event shall the Royal Society of Chemistry be held responsible for any errors or omissions in this *Accepted Manuscript* or any consequences arising from the use of any information it contains.



## Todorokite-type manganese oxide nanowires as an intercalation cathode for Li-ion and Na-ion batteries

B. W. Byles,<sup>a</sup> P. West,<sup>a</sup> D. A. Cullen,<sup>b</sup> K. L. More<sup>c</sup> and E. Pomerantseva<sup>\*a</sup>

Received 00th January 20xx,  
Accepted 00th January 20xx

DOI: 10.1039/x0xx00000x

www.rsc.org/

Extended hydrothermal treatment at an elevated temperature of 220° C allowed high yield synthesis of manganese oxide nanowires with a todorokite crystal structure suitable for ion intercalation. The flexible, high aspect ratio nanowires are 50–100 nm in diameter and up to several microns long, with 3x3 structural tunnels running parallel to the nanowire longitudinal axis. The tunnels are occupied by magnesium ions and water molecules, with the chemical composition found to be  $\text{Mg}_{0.2}\text{MnO}_2 \cdot 0.5\text{H}_2\text{O}$ . The todorokite nanowires were, for the first time, electrochemically tested in both Li-ion and Na-ion cells. A first discharge capacity of 158  $\text{mAh g}^{-1}$  was achieved in a Na-ion system, which was found to be greater than the first discharge capacity in a Li-ion system (133  $\text{mAh g}^{-1}$ ). Despite large structural tunnel dimensions, todorokite showed a significant first cycle capacity loss in a Na-ion battery. After 20 cycles, the capacity was found to stabilize around 50  $\text{mAh g}^{-1}$  and remained at this level for 100 cycles. In a Li-ion system, todorokite nanowires showed significantly better capacity retention with 78% of its initial capacity remaining after 100 cycles. Rate capability tests also showed superior performance of todorokite nanowires in Li-ion cells compared to Na-ion cells at higher current rates. These results highlight the differences in electrochemical cycling behavior of Li-ion and Na-ion batteries for a host material with spacious 3x3 tunnels tailored for large  $\text{Na}^+$  ions intercalation.

### Introduction

Na-ion batteries have received widespread attention as alternative energy storage devices to Li-ion batteries due to the vast abundance of sodium (constitutes 2.83% of the earth's crust compared to 0.0007% for lithium), the low cost of raw materials (~\$150 per ton of trona compared to ~\$5000 per ton of lithium carbonate), and many similarities between Na-ion and Li-ion electrochemical systems<sup>1–6</sup>. Most importantly, the mechanism of charge storage in both systems is based on the intercalation and diffusion of monovalent charge-carrying ions, which implies that Na-ion battery technology could be easily incorporated into current battery manufacturing processes. As a result, sodium-containing analogs of common Li-ion battery materials have been widely explored as Na-ion battery electrodes<sup>1–5</sup>. However, the major differences of using  $\text{Na}^+$  as a charge-carrier are that it is larger (1.06 Å cation radius versus 0.76 Å for  $\text{Li}^+$ ) and heavier (23  $\text{g mol}^{-1}$  atomic mass versus 6.9  $\text{g mol}^{-1}$  for lithium). This difference in size and weight limits the diffusion of ions through the crystal structure of an electrode host material. This results in significant capacity loss after the first cycle, poor cycle life, poor behavior at high current rates, and mechanical degradation of the electrode host material<sup>1–5</sup>.

Despite these challenges, Na-ion batteries are very attractive for large-scale applications where material price is of particular importance and energy per weight or footprint is less significant, such as grid level storage or load leveling applications where large battery systems are required and volume and weight constraints are not necessarily a concern<sup>1–5</sup>.

In order to enable reversible  $\text{Na}^+$  ions intercalation, the host structure should be able to accommodate  $\text{Na}^+$  ions without blocking their diffusion. Materials with layered crystal structures have been shown to exhibit facilitated diffusion behavior<sup>1</sup>. For example, layered compounds such as  $\text{NaCrO}_2$ ,  $\text{Na}_x\text{MnO}_2$ ,  $\text{NaNi}_{0.5}\text{Mn}_{0.5}\text{O}_2$ , and  $\text{Na}_{0.45}\text{Ni}_{0.22}\text{Co}_{0.11}\text{Mn}_{0.66}\text{O}_2$  have shown reversible capacities on the order of 100 to 150  $\text{mAh g}^{-1}$ <sup>1</sup>. However, these layered compounds face challenges such as low operating voltages, long term stability of the host crystal structure, and high polarization issues<sup>1</sup>. Materials with three-dimensional  $\text{Na}^+$  ion diffusion pathways, such as olivine-structured materials and NASICON (Na super ionic conductor) compounds, have also been explored for use in Na-ion batteries. These materials have shown reversible capacities greater than 100  $\text{mAh g}^{-1}$ , but due to intrinsic low electronic conductivities, these materials often exhibit slow kinetics unless coated with conductive additives<sup>3,5</sup>. An alternative to layered and three-dimensional structured electrode compounds are materials with tunnel crystal structures. For example, a tunnel manganese oxide,  $\text{Na}_{0.44}\text{MnO}_2$  ( $\text{Na}_4\text{Mn}_9\text{O}_{18}$ ), demonstrated a reversible capacity of 128  $\text{mAh g}^{-1}$  in a Na-ion battery<sup>4</sup>.

Todorokite-type manganese oxide, another tunnel-structured material, is of particular interest for use in Na-ion

<sup>a</sup> Department of Materials Science and Engineering, Drexel University, Philadelphia, PA 19104, USA.

<sup>b</sup> Materials Science and Technology Division, Oak Ridge National Laboratory, Oak Ridge, TN 37831, USA.

<sup>c</sup> Center for Nanophase Materials Sciences, Oak Ridge National Laboratory, Oak Ridge, TN 37831, USA.

batteries. This material has a large open tunnel crystal structure that provides enough space for  $\text{Na}^+$  ion intercalation and diffusion. The crystal structure of todorokite is built by  $\text{MnO}_6$  octahedra forming  $3 \times 3$  tunnels with a side length of  $9.5 \text{ \AA}$  (Fig. 1a).  $\text{Mg}^{2+}$  ions and water molecules are known to reside in the structural tunnels and stabilize such open crystallographic framework<sup>7</sup>. The size of charge-carrying  $\text{Li}^+$  and  $\text{Na}^+$  ions are shown alongside the schematic in Figure 1a, illustrating the relatively large volume available in the crystal tunnels for ions intercalation. Although this material has been explored as a cathode material in Li-ion systems<sup>8-12</sup>, Mg-ion system<sup>13</sup>, and Zn-ion system<sup>14</sup>, to the best of our knowledge, electrochemical intercalation of  $\text{Na}^+$  ions into todorokite has not been reported. In addition, reports on past use of todorokite as a battery electrode have either not reported the morphology<sup>8, 10, 11, 13</sup>, used a material with a platelet morphology<sup>12, 14</sup>, or used a mixed morphology of rods and platelets<sup>9</sup>. In this work, we use a simple hydrothermal procedure to synthesize todorokite-type manganese oxide with a flexible, one-dimensional nanowire morphology and for the first time report the performance of the todorokite nanowires in Li-ion and Na-ion battery electrodes.

## Experimental

The precursor material used to synthesize todorokite, layered buserite-structured manganese oxide, was prepared from Nabirnessite using a process described elsewhere<sup>15</sup>. In short, 50 mL of 1M  $\text{H}_2\text{O}_2$  and 50 mL of 0.5 M NaOH were combined and then added to a 50 mL solution of 0.3 M  $\text{Mn}(\text{NO}_3)_2$  under stirring. The resulting solution was allowed to react for one hour at room temperature, after which the precipitate, Na-birnessite manganese oxide, was filtered and thoroughly washed with deionized water. The Nabirnessite powder was then placed into a 1 L solution of 1M  $\text{MgCl}_2$  and stirred for 24 hours at a moderate stirring rate to perform an ion exchange and replace  $\text{Na}^+$  ions with  $\text{Mg}^{2+}$  ions, which is accompanied by a transformation of the birnessite phase to the buserite phase. Afterwards, the precipitate was filtered, washed with deionized water, and dispersed in a new 1 L solution of 1M  $\text{MgCl}_2$ . This process was repeated one more time for a total of three 24-hour ion exchanges, every time in fresh 1M  $\text{MgCl}_2$  solutions, resulting in the formation of Mg-buserite manganese oxide. The product was washed, filtered and dried at  $85^\circ\text{C}$  in air for 24 hours.

Todorokite-type manganese oxide was obtained by dispersing 50 mg of buserite powder in 17 mL of a 1M  $\text{MgCl}_2$  solution. This mixture was then placed in a 23 mL Teflon-lined stainless steel autoclave and hydrothermally treated for 1-4 days at  $180\text{--}220^\circ\text{C}$ . The final products were filtered, washed, and dried at  $100^\circ\text{C}$  for 12 hours.

Phase analysis was performed using a Rigaku SmartLab X-Ray Diffractometer (Japan) with  $\text{Cu K}\alpha$  radiation over a typical range of  $5\text{--}40^\circ 2\theta$  with a step size of  $0.02^\circ$ . The morphology and chemical composition of the materials were investigated using a Zeiss Supra 50VP (Germany) scanning electron microscope (SEM) equipped with an energy dispersive X-ray spectroscopy (EDS) attachment. Atomic resolution high-angle annular dark-field scanning transmission electron microscopy (HAADF-STEM) images were recorded using an aberration-corrected Nion UltraSTEM 100 operated at 100kV. Energy dispersive X-ray analysis (EDS) was performed on a JEOL

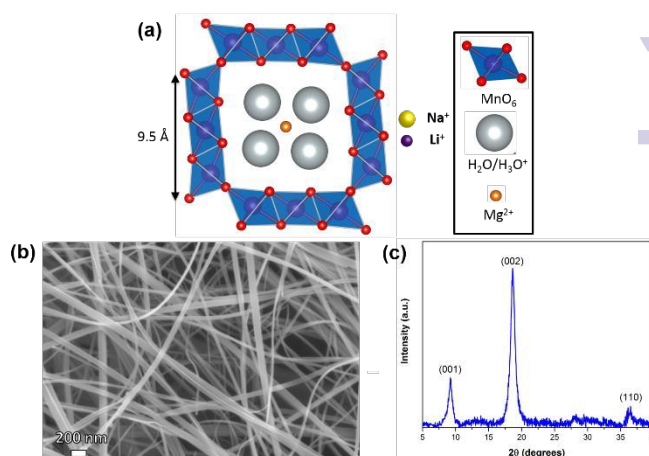


**Figure 1.** (a) Schematic of  $\text{Mg}_{0.20}\text{MnO}_2 \cdot x\text{H}_2\text{O}$  todorokite crystal structure with the relative sizes of charge carrying ions. Oxygen ions (red) are not to scale. (b) SEM image and (c) XRD pattern of high aspect ratio todorokite nanowires.

JEM2200FS equipped with a  $30 \text{ mm}^2$  Bruker silicon drift detector (SDD). Collected spectra were quantified using the standardless Cliff-Lorimer ratio technique for thin foil X-ray microanalysis built into the Bruker Esprit software. Thermal gravimetric analysis was performed on a Perkin-Elmer TGA 7 at a heating rate of  $10^\circ\text{C}/\text{min}$  in air from room temperature up to  $800^\circ\text{C}$ .

Electrodes of todorokite nanowires were fabricated using a doctor's blade method to cast a slurry consisting of 70% active material, 20% acetylene black conductive agent, and 10% poly(vinylidene fluoride) (PVDF) binder dispersed in 1-methyl-2-pyrrolidinone (NMP) onto an Al foil current collector. Electrodes were dried at  $100^\circ\text{C}$  for 12 hours under vacuum before transferring into an Ar-filled glovebox. Two-electrode coin cells (2016 type) were assembled for electrochemical testing of the manganese oxides in a half-cell configuration. Lithium foil and sodium metal were used as both the counter and reference electrodes for Li-ion and Na-ion cells respectively. The electrolyte solution for Li-ion cells was 1M  $\text{LiPF}_6$  dissolved in a mixture of ethylene carbonate (EC) and diethyl carbonate (DEC) with a 1:1 volume ratio. For the Na-ion cells, the electrolyte was 1M  $\text{NaClO}_4$  dissolved in propylene carbonate (PC) with a 5 vol. % fluoroethylene carbonate (FEC) additive. Cyclic voltammetry (CV) curves were recorded using a VMP3 potentiostat/galvanostat (BioLogic, France) at a scan rate of  $0.1 \text{ mV s}^{-1}$ . Galvanostatic cycling was performed at various C-rates using a battery testing station (Arbin Instruments, USA). The potential ranges for todorokite were 2.0-4.2 V vs Li/Li<sup>+</sup> for the Li-ion cells and 1.6-3.6 V vs Na/Na<sup>+</sup> for the Na-ion cells. All solid chemicals were obtained from Alfa Aesar, and the electrolyte solvents and additives were produced by Aldrich and Novolyte.

## Results and discussion

Figure 1b shows the morphology of todorokite nanowires synthesized via hydrothermal treatment of Mg-buserite in 1M  $\text{MgCl}_2$  solution at  $220^\circ\text{C}$  for 4 days. These high aspect ratio one-dimensional crystals have diameters of 50-100 nm and lengths of up to several microns. The entangled nanowires also appear to be very flexible

and demonstrate significant bending without breaking. Figure 1c shows the XRD pattern for the synthesized todorokite, which is in agreement with the previous reports<sup>15-18</sup>. The XRD pattern of todorokite shows peaks in the same locations ( $2\theta = 8^\circ$  and  $18^\circ$ ) as its precursor material, Mg-buserite, but the change in the ratio of the intensity of the (002) peak to the (001) peak indicates that the tunnel-structured todorokite (space group P2/m) has formed from the layered Mg-buserite precursor<sup>15</sup>. There has been a single previous report on the formation of todorokite-structured nanowires<sup>16</sup>, where the authors used a similar synthesis approach involving ion exchange and hydrothermal treatment. However, they began the procedure with a more complicated sol-gel process involving organic molecules and did not use their nanowires in any type of electrochemical energy storage system. Their nanowires were of similar dimensions compared to the ones obtained in our work, but they possessed more  $\text{Mg}^{2+}$  ions in the structure with the reported composition of  $\text{Mg}_{0.35}\text{Mn}_{0.91}\text{O}_2 \cdot x\text{H}_2\text{O}$ . From the EDS data, it was determined that Mg/Mn ratio in our todorokite nanowires is  $\sim 0.2$ , and the lower amount of magnesium ions allows for more charge-carrying ions to be electrochemically inserted into the structure.

In order to investigate the mechanism of todorokite nanowire formation, hydrothermal treatment of Mg-buserite was performed at various temperatures and stopped after different lengths of time. Figure 2 shows SEM images of the materials obtained in these experiments. When hydrothermal treatment at  $180^\circ\text{C}$  was stopped after 24 hours, the product showed a mixture of micron-sized platelets and rods (Fig. 2a). When the synthesis temperature was increased to  $220^\circ\text{C}$  and the length of hydrothermal treatment increased to 48 hours, nanowires of todorokite began to grow via the splitting of the platelets into multiple flexible fibers, which can be seen in Figure 2b. Subsequent increase of synthesis time to 4 days

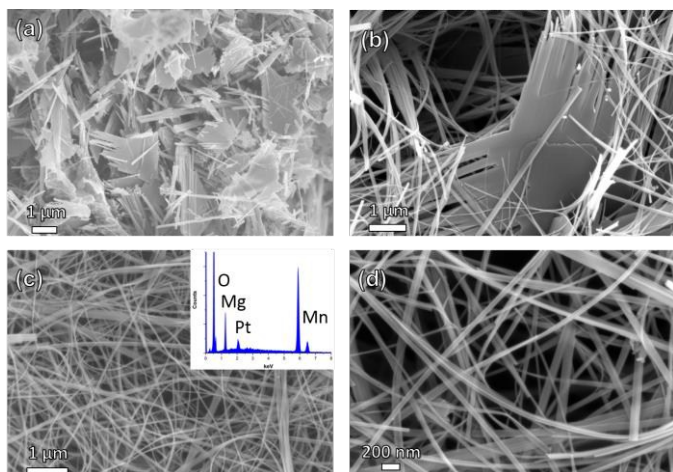


**Figure 2.** SEM images of (a) todorokite platelets and nanowires after 24 hours of hydrothermal treatment at  $180^\circ\text{C}$ , (b) todorokite platelet splitting into nanowires after 48 hours of hydrothermal treatment at  $220^\circ\text{C}$ , and (c) low magnification and (d) high magnification SEM images of todorokite nanowires resulting from hydrothermally treatment for 4 days at  $220^\circ\text{C}$ , demonstrating high yield of pure nanowire morphology. Inset in (c) shows representative EDS spectrum for todorokite nanowires. Pt peak is due to sputter coating of SEM sample.

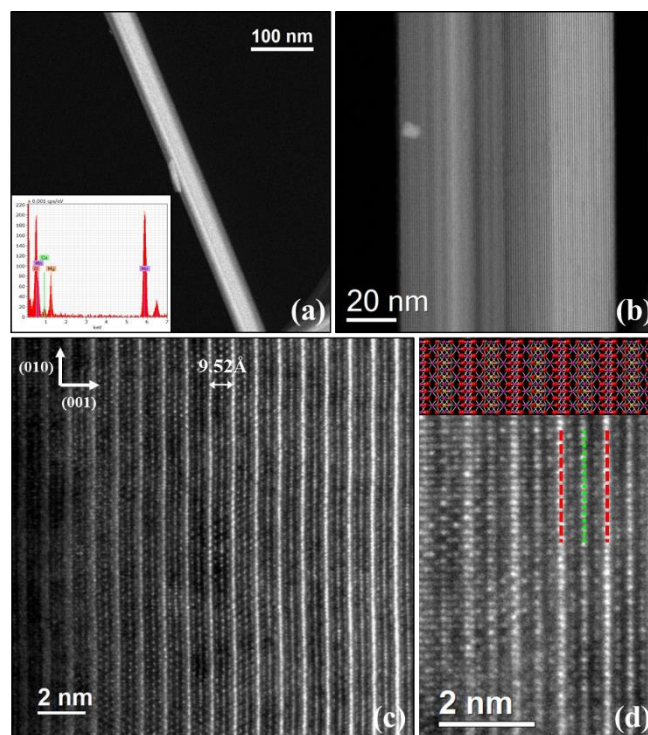


**Figure 3.** Aberration-corrected HAADF-STEM images of todorokite nanowires. (a) Single nanowire with inset EDS spectrum. (b) Lattice image of nanowire showing the (001) spacing. (c) Atomic resolution image showing tunnels as viewed along the [100] direction. (d) Atomic resolution image showing position of tunnels (red dashed line: tunnel walls, green dotted line: tunnel center) with overlaid ball-and-stick model of todorokite (red: O, magenta: Mn, orange: Mg, gray:  $\text{H}_2\text{O}$ ).

resulted in a high yield of pure todorokite nanowires, shown in Figures 2c and 2d. The nanowire morphology of materials generally shows better mechanical stability in reversible ions intercalation, enabling longer lifetime of the battery.

Further structural and compositional analysis of the pure todorokite nanowires was performed using aberration-corrected STEM analysis. The HAADF-STEM images presented in Figure 3 confirm the todorokite tunnel structure previously determined by XRD. Figure 3b shows a single todorokite wire oriented along the [100] direction relative to the electron beam. The brightest lattice planes in the atomic resolution images in Figure 3c,d correspond to rows and columns of pure Mn atoms which constitute the tunnel framework. Three other lattice planes are observed between the bright planes, the middle plane marking the center of the tunnel systems. The Mg atoms reside in the atomic columns along this plane. The other two planes originate from Mn atoms in the cross framework of the tunnels. Due to lower atomic number, oxygen and hydrogen atoms contribute much lower overall contrast in the Z-contrast HAADF images and thus the oxygen and water planes are not readily visible.

The TGA profile for the todorokite nanowires is illustrated in Figure 4. This curve is in agreement with previously reported results<sup>8, 9, 14-16</sup>. The 1 wt. % loss from room temperature to  $\sim 250^\circ\text{C}$  is attributed to the evaporation of physically adsorbed surface water.

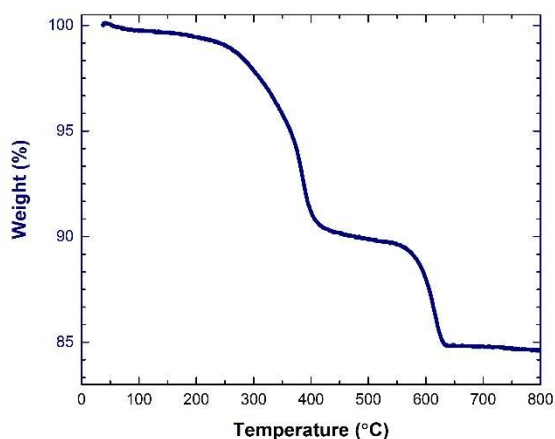


**Figure 4.** TGA curve obtained for todorokite-type manganese oxide nanowires in air.

The 9% drop in weight from  $\sim 250\text{--}380^\circ\text{C}$  results from the dehydration of structural water residing in the tunnel space. The sharp decrease in weight at  $600^\circ\text{C}$  corresponds to the evolution of oxygen and decomposition of the todorokite structure to  $\text{Mn}_3\text{O}_4$ .

From the weight loss beginning at  $250^\circ\text{C}$ , the amount of structural water was found to be 0.5 molecules of  $\text{H}_2\text{O}$  per  $\text{MnO}_2$  unit. Combined with EDS data (inset Figure 2c), the chemical formula for the todorokite was found to be  $\text{Mg}_{0.20}\text{MnO}_2 \cdot 0.5\text{H}_2\text{O}$ . Structural water is believed to play an important role in facilitating the insertion of larger or multivalent ions into a crystal structure due to the fact that it can provide charge screening and minimize the electrostatic interactions between the host structure anions and the intercalating cation, assist in maintaining an open crystal structure with repeated insertion/deinsertion cycles and, in manganese oxides, help suppress  $\text{Mn}^{2+}$  dissolution<sup>19–23</sup>.

Figure 5 shows the electrochemical performance of todorokite nanowires in Li-ion and Na-ion batteries. The CV curves for todorokite in a Li-ion and Na-ion systems are shown in Figures 5a and 5b, respectively. Both CV curves demonstrate large redox peaks indicative of typical ion insertion type behavior. The CV for todorokite in a Li-ion battery shows a pair of corresponding redox peaks at 2.56 V and 2.98 V. However, there is also a peak at 3.78 V on the first charge that disappears with subsequent cycling, and there is a shoulder on the anodic peak at 2.34 V that decreases in intensity with each cycle. These peaks can be attributed to irreversible  $\text{Li}^+$  insertion sites within the todorokite host<sup>8</sup>, and the shoulder peak at 2.34 V can be correlated to the existence of a second plateau in the galvanostatic discharge curves in Figure 5c. The CV curve for the Na-ion system (Fig. 5b) shows a single pair of redox peaks at 1.93 V and 2.38 V, indicating a single insertion site. The intensity of these peaks decreases after the first cycle, consistent with galvanostatic cycling data showing a loss in capacity from the irreversibility of the initial sodium insertion. The smaller decrease in magnitude of the intensity of the two major redox peaks for the lithium system compared to the sodium indicates much better initial capacity retention of todorokite in Li-ion batteries. Further, in both lithium and sodium systems, the redox peaks shift to more positive values upon cycling. This has been observed for other manganese oxide phases and has been attributed to local restructuring and solid electrolyte interphase (SEI) formation<sup>24</sup>.

Galvanostatic discharge/charge curves for todorokite in both battery systems are shown in Figures 5c and 5d. Upon first discharge, todorokite exhibits a higher capacity of  $158\text{ mAh g}^{-1}$  in a Na-ion system compared to  $133\text{ mAh g}^{-1}$  in a Li-ion system. The difference between the two battery systems may be due to the fact that the large open tunnel structure has more favorable insertion sites for sodium. However, upon first charge, much less sodium was extracted from the todorokite structure than was inserted, with a first charge capacity of  $82\text{ mAh g}^{-1}$ . The Li-ion system, on the other

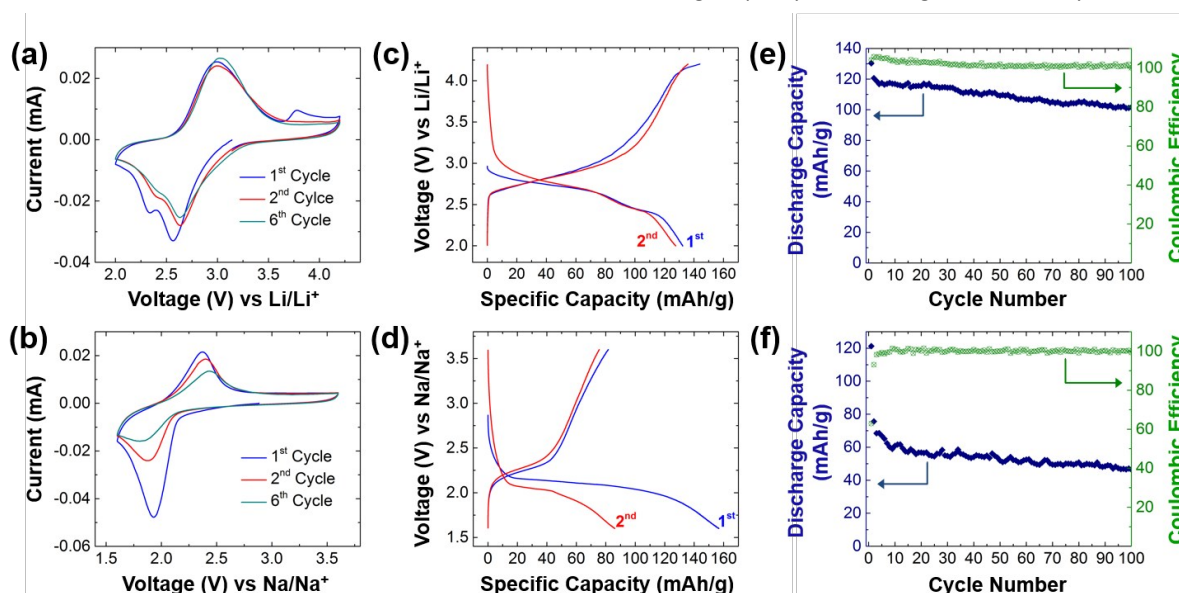


**Figure 5.** Electrochemical performance of todorokite-type manganese oxide nanowires in Li-ion (a, c, e) and Na-ion batteries (b, d, f) (a, b) CV curves recorded at a sweep rate of  $0.1\text{ mV s}^{-1}$  (c, d) first and second discharge/charge cycles for todorokite manganese oxide at a rate of  $C/50$ . (e, f) Extended cycling plots of todorokite manganese oxide at  $C/10$  rate showing coulombic efficiency.

hand, exhibited much better reversibility during the first cycle (Fig. 5c). For both systems, the largest capacity drop is seen from the first to second cycle, with the Na-ion system showing a greater decrease in capacity. This large first cycle capacity loss is a common occurrence for Na-ion battery electrode materials<sup>1-5</sup>. In the case of todorokite, the loss may be due to ions initially inserted on the first discharge becoming trapped and held as stabilizing ions by the todorokite structure, a phenomenon that has been reported in the past for other tunnel-structured manganese oxides in Li-ion systems<sup>25</sup>. This mechanism of capacity loss can be even more pronounced for Na-ion system because of diffusion limitations of the larger and heavier ions. Further, it has been suggested in the past that Li<sup>+</sup> ions may become trapped in the 1x1 tunnels located at the corners of the larger 3x3 todorokite crystal tunnels<sup>8</sup>. This process may also be occurring with Na<sup>+</sup> ions, as past reports demonstrated the insertion of these large ions into  $\beta$ -MnO<sub>2</sub> with 1x1 tunnels<sup>26,27</sup>.

Extended cycling data for todorokite in both systems is shown in Figures 5e and 5f. After 100 cycles at a C/10 current rate, todorokite has a higher capacity retention of 78% of its initial discharge capacity in the Li-ion system compared to 38% of its initial discharge capacity in the Na-ion system. For the Li-ion system, the capacity remains relatively constant after the first 5 cycles with only a small decrease in capacity with further cycling, and the same is true for the Na-ion system after 15 cycles. The loss of capacity with extended cycling has also been attributed to multiple phenomena in the past for manganese oxides in both Li-ion and Na-ion batteries, including the dissolution of Mn<sup>2+</sup> into the electrolyte solution, displacement of Mn<sup>3+/4+</sup> and O<sup>2-</sup> ions from the tunnel walls to stabilize the structure, and Jahn-Teller distortions in MnO<sub>6</sub> octahedra that occur when the oxidation state of manganese falls below a critical value<sup>1,28</sup>.

Figure 6 shows rate capability data for todorokite nanowires in both Li-ion and Na-ion battery systems. In a Li-ion battery, the nanowires maintain 91% of their first discharge capacity at a C/10 rate, 72% at a C/2 rate, and 59% of their first discharge capacity at a 1C rate. In the Na-ion system, todorokite maintains 41% of its first discharge capacity at a C/10 rate, 19% at a C/2 rate, and 12% at a 1C rate. In both battery types, capacity recovers when a current corresponding to the initial C/20 rate is applied again after 20 cycles. In the Li-ion system, the nanowires recover nearly 100% of initial discharge capacity, while in the Na-ion system, the nanowires recover 49% of initial capacity. However, if the capacity at the second application of the C/20 rate in a Na-ion battery is compared to second overall discharge cycle (after irreversible first cycle capacity losses), todorokite nanowires recover 83% of this capacity. We believe that the todorokite exhibits higher capacities at higher C-

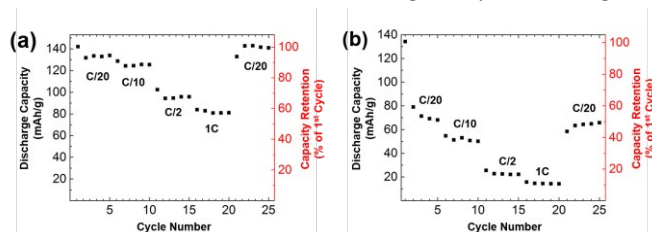


**Figure 6.** Rate capability and capacity retention of todorokite nanowires at different current rates in (a) Li-ion cell and (b) Na-ion cell.

rates in the Li-ion system compared to the Na-ion system due to the kinetic limitations of Na<sup>+</sup> compared to Li<sup>+</sup>.

The electrochemical performance of todorokite nanowires shows improvements compared to past reports for todorokite-structured materials with different morphologies in Li-ion cells<sup>8-12</sup>. Similar capacities in the range of 120-160 mAh g<sup>-1</sup> have been achieved, but all of the previous reports showed more severe first cycle capacity loss and/or poorer capacity retention up to 30 cycles. Additionally, no work has shown either extended cycling behavior beyond 30 cycles or the performance of todorokite at higher current rates. The smaller first cycle capacity loss, better capacity retention, and rate capability performance of our todorokite could be attributed to the nanowire morphology of the material.

Although there have been no other reports on the electrochemical insertion of Na<sup>+</sup> ions into todorokite, its performance can be compared to another tunnel-structured manganese oxide material with a nanowire morphology, Na<sub>0.44</sub>MnO<sub>2</sub> (Na<sub>4</sub>Mn<sub>9</sub>O<sub>18</sub>). This material possesses S-shaped tunnels active for reversible sodium cycling and considered to be one of the most promising cathode materials for Na-ion batteries<sup>29</sup>. Na<sub>0.44</sub>MnO<sub>2</sub> nanowires have exhibited a reversible capacity of 128 mAh g<sup>-1</sup> in a Na-ion cells without a large first cycle capacity loss, and it maintained a large percentage of its initial capacity at higher current rates (>100 mAh g<sup>-1</sup> at 8.3C)<sup>29</sup>. Investigation of Na<sub>0.44</sub>MnO<sub>2</sub> phase has demonstrated that materials with tunnel crystal structures can be used for reversible intercalation/deintercalation of Na<sup>+</sup> ions with much smaller capacity losses than what we observed for todorokite-structured manganese oxide, even at higher current rates. Although Na<sub>0.44</sub>MnO<sub>2</sub> nanowires possess a different tunnel configuration with different stabilizing cations, it is built from the same MnO<sub>6</sub> octahedra building blocks as the todorokite structure. Therefore, it should be possible to achieve improved performance of todorokite in Na-ion batteries in terms of decreasing first cycle capacity loss and increasing capacity retention. Finding a solution to the issues that todorokite has demonstrated in Na-ion batteries requires development of creative strategies to mitigate capacity loss, such as extraction of Mg<sup>2+</sup> ions and chemical preintercalation of Na<sup>+</sup> ions to stabilize the crystal structure of todorokite and decrease the first cycle capacity loss.

As evidenced by the differences in performance of todorokite in two types of ion insertion batteries, it is apparent that materials used in Na-ion batteries cannot be simply considered analogous to those used in Li-ion batteries. Even though Li<sup>+</sup> and Na<sup>+</sup> ions are characterized by the same charge and similar electrochemical potentials, their insertion and diffusion behavior can vary dramatically. Todorokite possesses a large open crystal structure capable of intercalating both Li<sup>+</sup> and Na<sup>+</sup> ions, and although the size and mass of the two ions are different, this should not play a significant role at very low current rates. However, there is still a significant difference in the performance of the material in each respective type of battery. It is therefore very important to develop a thorough understanding of the relationship between the properties of different charge-carrying ions and the crystal structure and composition of a host material.

## Conclusions

Todorokite nanowires with diameters of 50-100 nm and up to several microns long were synthesized via a facile hydrothermal process. For the first time, this material with large 3x3 tunnels was used as an intercalation host for the electrochemical insertion of sodium, and its novel nanowire morphology was also cycled for the first time in Li-ion batteries. A higher first discharge capacity of 158 mAh g<sup>-1</sup> is reported in a Na-ion system, compared to 133 mAh g<sup>-1</sup> for the Li-ion system. Further, after an initial capacity drop, the capacity of todorokite in a Na-ion system stabilizes with cycling. Despite possessing a large amount of open crystal tunnel space for Na<sup>+</sup> intercalation, todorokite faces electrochemical performance challenges typical for Na-ion battery materials. Therefore, it is important to note that intercalation of charge-carrying ions is not simply a function of the amount of space available in the material, but rather is dependent on many other factors, including but not limited to the composition and water content of the material, the material morphology, and the stability of the host crystal structure. Future work should be aimed not only at improving the performance of todorokite through chemical modifications, but also at gaining a better understanding of the relationship between alternative charge-carrying ions insertion and the host material's intrinsic chemical, electronic, mechanical, and structural properties. The ability to intercalate different charge-carrying ions makes todorokite nanowires an attractive material for future investigation in numerous electrochemical applications, and the materials' flexible morphology gives it potential to function as a freestanding membrane for electrochemical and ion absorption applications.

## Acknowledgements

This work was supported by Drexel University start-up funds. We would like to acknowledge Drexel's Centralized Research Facilities for assistance in materials characterization, and Prof. Yury Gogotsi and the AJ Drexel Nanomaterials Institute for their help and support. We would also like to acknowledge Prof. Christopher Li and Ziyin Huang from the Soft Materials Group at Drexel University for carrying out TGA experiments. STEM analysis was performed through a user project supported by ORNL's Center for Nanophase Materials Sciences (CNMS), which is a Dept. of Energy, Office of Science User Facility.

## Notes and references

- M. H. Han, E. Gonzalo, G. Singh and T. Rojo, *Energy & Environmental Science*, 2015, **8**, 81-102.
- S.-W. Kim, D.-H. Seo, X. Ma, G. Ceder and K. Kang, *Advanced Energy Materials*, 2012, **2**, 710-721.
- D. Kundu, E. Talaie, V. Duffort and L. F. Nazar, *Angewandte Chemie International Edition*, 2015, **54**, 3431-3448.
- M. D. Slater, D. Kim, E. Lee and C. S. Johnson, *Advanced Functional Materials*, 2013, **23**, 947-958.
- N. Yabuuchi, K. Kubota, M. Dahbi and S. Komaba, *Chemical Reviews*, 2014, **114**, 11636-11682.
- R. E. Krebs, *The History and Use of Our Earth's Chemical Elements: A Reference Guide*, Greenwood Press, 1998.
- J. E. Post, P. J. Heaney and J. Hanson, *American Mineralogist*, 2003, **88**, 142-150.
- M. J. Duncan, F. Leroux, J. M. Corbett and L. F. Nazar, *Journal of The Electrochemical Society*, 1998, **145**, 3746-3757.
- N. Kumagai, S. Komaba, K. Abe and H. Yashiro, *Journal of Power Sources*, 2005, **146**, 310-314.
- Y. Yang, D. Shu, J. K. You and Z. G. Lin, *Journal of Power Sources*, 1999, **81-82**, 637-641.
- Y. Yang, D. Shu, H. Yu, X. Xia and Z. G. Lin, *Journal of Power Sources*, 1997, **65**, 227-230.
- H.-J. Cui, J.-W. Shi, F. Liu and M.-L. Fu, *Journal of Materials Chemistry*, 2011, **21**, 18527-18529.
- N. Kumagai, S. Komaba, H. Sakai and N. Kumagai, *Journal of Power Sources*, 2001, **97-98**, 515-517.
- J. Lee, J. B. Ju, W. I. Cho, B. W. Cho and S. H. Oh, *Electrochimica Acta*, 2013, **112**, 138-143.
- Q. Feng, H. Kanoh, Y. Miyai and K. Ooi, *Chemistry of Materials*, 1995, **7**, 1722-1727.
- J. Liu, J. Cai, Y.-C. Son, Q. Gao, S. L. Suib and M. Aindow, *The Journal of Physical Chemistry B*, 2002, **106**, 9761-9768.
- A. Onda, S. Hara, K. Kajiyoshi and K. Yanagisawa, *Applied Catalysis A: General*, 2007, **321**, 71-78.
- Y. F. Shen, R. P. Zenger, R. N. DeGuzman, S. L. Suib, L. McCurdy, D. I. Potter and C. L. O'Young, *Science*, 1993, **260**, 511-515.
- E. Beaudrouet, A. Le Gal La Salle and D. Guyomard, *Electrochimica Acta*, 2009, **54**, 1240-1248.
- K. W. Nam, S. Kim, S. Lee, M. Salama, I. Shterenberg, Y. Gofer, J.-S. Kim, E. Yang, C. S. Park, J.-S. Kim, S.-S. Lee, W.-S. Chang, S.-G. Doo, Y. N. Jo, Y. Jung, D. Aurbach and J. W. Choi, *Nano Letters*, 2015, **15**, 4071-4079.
- K. W. Nam, S. Kim, E. Yang, Y. Jung, E. Levi, D. Aurbach and J. W. Choi, *Chemistry of Materials*, 2015, **27**, 3721-3725.
- J. Song, M. Noked, E. Gillette, J. Duay, G. Rubloff and S. B. Lee, *Physical Chemistry Chemical Physics*, 2015, **17**, 5256-5264.
- Q. Wei, J. Liu, W. Feng, J. Sheng, X. Tian, L. He, Q. An and L. Mai, *Journal of Materials Chemistry A*, 2015, **3**, 8070-8075.
- C. Zhang, C. Feng, P. Zhang, Z. Guo, Z. Chen, S. Li and H. Liu, *RSC Advances*, 2012, **2**, 1643-1649.
- C. S. Johnson, D. W. Dees, M. F. Mansuetto, M. M. Thackeray, D. R. Vissers, D. Argyriou, C. K. Loong and L. Christensen, *Journal of Power Sources*, 1997, **68**, 570-577.
- D. Su, H.-J. Ahn and G. Wang, *Journal of Materials Chemistry A*, 2013, **1**, 4845-4850.
- D. Su, H.-J. Ahn and G. Wang, *NPG Asia Mater*, 2013, **5**, e70.
- M. M. Thackeray, *Progress in Solid State Chemistry*, 1997, **25**, 1-71.
- E. Hosono, T. Saito, J. Hoshino, M. Okubo, Y. Saito, D. Nishio-Hamane, T. Kudo and H. Zhou, *Journal of Power Sources*, 2012, **217**, 43-46.

## Graphical Abstract

